RSC Advances

PAPER

View Article Online
View Journal | View Issue

Cite this: *RSC Adv.*, 2023, **13**, 27283

Pd nanoparticles decorated ultrathin 2D metal–organic framework nanosheets with enhanced peroxidase–mimic activity and colorimetric assay of glucose†

Ying Shen, *[a] Hongyuan Wu,[b] Xia Luo,[a] Haizhi Zhang *[b] and Liming Cheng*[a]

In addition to size, shape and morphology, enzyme–mimetic property could be efficiently regulated by controlling composition, forming complexes or hybrids, and surface modification. Herein, Pd nanoparticles with an average diameter of 2.52 nm were decorated on ultrathin 2D copper(II)-porphyrin derived metal–organic framework (MOF) nanosheets by a simple reduction method for catalytic activity regulation. In comparison with other nanozymes, the as-synthesized Pd modified 2D MOF hybrid nanosheets (Pd@Cu-TCPP(Fe)) presented excellent peroxidase–mimic activity, exhibiting an even superior catalytic ability towards H_2O_2 with a Michaelis–Menten constant as low as 2.33 mM. Based on a cascade reaction between glucose oxidase and Pd@Cu-TCPP(Fe), a colorimetric method for the detection of glucose was established and validated with a wide linear range (0.2–8.0 mM), good recovery (89.5–94.2%) and nice reproducibility (3.65%). All these features guaranteed its excellent ability for glucose determination in human cerebrospinal fluids. This study could offer a valuable reference for constructing novel optical biosensors.

Received 27th July 2023
Accepted 5th September 2023

DOI: 10.1039/d3ra05072f

rsc.li/rsc-advances

Introduction

Rapid detection of various compounds based on biosensors is essential in different fields including clinical diagnosis, agricultural product quality control, food safety and environmental monitoring.[1–5] In comparison with other analytical techniques depending on large instruments, biosensors have gained great attention due to their convenience. Natural enzymes as important bio-receptors or labels in biosensors are always expensive, due to the difficulty in their preparation and purification.[6] Moreover, their catalytic activity is always apt to decrease over time when exposed to extreme temperature or pH. As a result, nanomaterial-based enzymes with intrinsic enzyme–mimic activity, namely nanozymes, have been demonstrated to be satisfying substitutes of natural enzymes resulting from their high stability, low-cost and simple preparation. Up to now, large numbers of nanozymes as promising candidates have been widely used from sensing to therapeutics.[7–12] Thus, searching for high-activity bioinspired nanozymes has become a hot topic in the field of analytical chemistry and material science.

As a typical kind of nanozymes, metal–organic frameworks (MOFs) have gained prodigious appreciation in the construction of various biosensors. MOFs, an emerging class of porous materials constructed from metal nodes and functional organic ligands, possess attractive characteristics, such as high porosity, large surface area and abundant enzyme active center, which make them regarded as star materials for enzyme mimics. A lot of research has been devoted to the development of MOF-based nanozymes as cheap and stable candidates.[13,14] However, most of these studies have focused on bulk MOFs where most of the active sites are hidden in the framework. Ultrathin two-dimensional (2D) MOF nanosheets, as one kind of new-developing nano-scale MOFs, have the advantages of both 2D materials as well as the unique properties of MOFs. They integrates merits of good conductivity, larger surface areas, abundant exposed active sites along with tailorable structures.[15–19] Recently, considerable efforts have been devoted by our group to develop 2D MOFs based sensors for agricultural products quality control.[20,21] Up to now, although some kinds of ultrathin 2D MOFs have been reported, such as MOF-5, 2D M-TCPP (M = Co, Cu, and Zn), b-CuBDC, MnDMS, Ni/Fe-MOF NSs, CoTCPP-py-Cu, and Zn/Ni-MOF-2 *et al.*,[22,23] 2D MOFs with high catalytic activity are limited. As a result, enzyme activity regulation is a good strategy to construct biomimetic enzymes based on 2D MOFs. In addition to tune size, shape and morphology, there are three main methods for activity regulation of nanozymes (controlling composition, forming

[a]*Department of Laboratory Medicine, Tongji Hospital, Tongji Medical College, Huazhong University of Science and Technology, Wuhan 430030, P. R. China. E-mail: sying830@163.com; chengliming2015@163.com*

[b]*College of Food Science and Engineering, Wuhan Polytechnic University, Wuhan 430023, China. E-mail: hzzhang@iccas.ac.cn*

† Electronic supplementary information (ESI) available. See DOI: https://doi.org/10.1039/d3ra05072f

complexes or hybrids, surface coating and modification).[24] Among these, constructing hybrids based on ultrathin 2D MOF have been seldomly explored except for doped with gold nanoparticles.[16,20] Therefore, it is highly desirable to explore new ultrathin 2D MOF hybrids with enhanced enzyme-mimetic activity for widespread practical application.

Palladium nanoparticles (PdNPs), as one kind of metallic nanoparticles (MNPs), are gaining great interest in wide range of biomedical applications owing to their high surface-to-volume ratio, broad catalytic properties, easy synthesis, and tunable surface functionalization.[25] Besides the general characteristics of MNPs, the noble PdNPs also exhibit unique properties, such as good chemical stability, high thermal stability, remarkable photocatalytic activity and electronic properties.[26] More importantly, PdNPs could be synthesized by an *in situ* method, which makes it suitable for the construction of nanocomposites or hybrid nanomaterials. So far, important progresses have been achieved in developing PdNPs-based nanozymes, such as Pd@Au, GSH-Pd nanoparticles, Pd@ZIF-8.[27–36] However, to the best of our knowledge, there have been few literature about PdNPs doped 2D MOF hybrids.

In this study, the copper(II)-porphyrin derived MOF nanosheets (Cu-TCPP(Fe)) was chosen for study. On one hand, tetra (4-carboxyphenyl) porphyrin (TCPP) based 2D MOFs could accelerate electron transfer due to the formed C–O-metal bond between TCPP and metal node which might be favor for biomimetic catalysis.[37] On the other hand, the 2D lamellar structure and the existence of the abundant carboxyl groups is beneficial to decorate PdNPs due to large surface area and carboxylate ligand to metal interaction. Then, PdNPs were modified on 2D Cu-TCPP(Fe) nanosheets by a simple *in situ* method under mild reaction condition. The obtained hybrid nanosheets (Pd@Cu-TCPP(Fe)) were fully characterized and their peroxidase–mimic activity was well studied. Furthermore, this nanozyme was coupled with glucose oxidase (GOx) to develop a sensing platform for selective detection of glucose. As a proof-of-concept application, the sensing strategy based on Pd@Cu-TCPP(Fe) hybrid nanosheets was used to determine glucose in human cerebrospinal fluids.

Experimental methods

Materials and reagents

Fe(III) *meso*-tetra (4-carboxyphenyl) porphyrin chloride (TCPP(Fe)) was purchased from Frontier Scientific (Logan, Utah, USA). Copper nitrate trihydrate ($Cu(NO_3)_2 \cdot 3H_2O$), trifluoroacetic acid (TFA) and sodium tetrachloropalladate (Na_2PdCl_4) were all obtained from Aladdin Biochemical Technology Co., Ltd (Shanghai, China). Poly-vinylpyrrolidone K30 (PVP) and sodium borohydride ($NaBH_4$) were both purchased from Sinopharm Chemical Reagent Co., Ltd (Shanghai, China). Hydrogen peroxide solution (H_2O_2, 30% w/w) was obtained from Damao Chemical Reagent Factory (Tianjin, China). Zinc sulfate heptahydrate ($ZnSO_4 \cdot 7H_2O$), glucose, glucose oxidase (GOx), lactose, sucrose, maltose, lysine (Lys), tryptophan (Trp) and homovanillic acid (HVA) were all purchased from Sigma-Aldrich Chemical Reagent Co., Ltd (St Louis, MO, USA). 3,3′,5,5′-Tetramethylbenzidine (TMB) were gotten from Shanghai Yuanye Bio-Technology Co., Ltd (Shanghai, China). Deionized water was prepared by a water purification system (Elga, England). All chemical reagents were available from commercial sources and used without further purification.

Apparatus

UV-vis absorption spectra were recorded on an Evolution 220 UV-vis spectrophotometer (Thermo Fisher, USA) using a quartz cell with 1 cm path length. Transmission electron microscopy (TEM) was carried out on the JEOL JEM 2100F equipment (JEOL, Japan) for morphology observation. All the average sizes were obtained by measuring more than 100 dispersive nanoparticles. The images of elements distribution were observed by the energy dispersive spectroscopy (EDS) on the JED2300 equipment (JEOL, Japan). X-Ray photoelectron spectroscopy (XPS) was performed on an ESCALAB Xi+ spectrometer (Thermo Fisher, USA) with monochrome Al K_α X-rays. Powder X-ray diffraction (PXRD) data were collected on a Rigaku SmartLab SE diffractometer using Cu K_α radiation (Japan). Atomic force microscopy (AFM) was performed using a Bruker Dimension Icon Microscope (Bruker, USA), and the samples were dispersed on a mica plate for the test. Fourier transform infrared (FTIR) spectroscopy was conducted on a Thermo IN10 FTIR microscope (Thermo Fisher, USA). Electron paramagnetic resonance spectra (EPR, EMXPLU-12) was recorded to detect $^{\bullet}OH$.

Preparation of Cu-TCPP(Fe) nanosheets

Cu-TCPP(Fe) nanosheets were prepared based on the previous report.[38] First, 2.4 mg of $Cu(NO_3)_2 \cdot 3H_2O$, 40.0 μL of TFA (1.0 M) and 10.0 mg of PVP were all added into a mixture solution of DMF and ethanol (v/v, 3 : 1) in a glass tube. Then, 4.4 mg of TCPP(Fe) was as well dissolved in a mixture of DMF and ethanol (v/v, 3 : 1), and this obtained mixture was slowly added into the aforementioned solution under stirring. At last, the above mixed solution was ultra-sounded for 20 min and then heated at 80 °C for 4 h. The resultant solution was centrifugated to obtain 2D MOF nanosheets, and the yield was about 62.1%. The nanosheets were washed twice with ethanol and redispersed in ultrapure water with a concentration of 1.0 mg mL^{-1} for further use.

Preparation of Pd@Cu-TCPP(Fe) hybrid nanosheets

Cu-TCPP(Fe) nanosheets prepared above were decorated with PdNPs. Typically, 10 mL of Na_2PdCl_4 solution (1.0 mg mL^{-1}) was added into 20 mL of Cu-TCPP(Fe) dispersion (7.5 mg mL^{-1}). After stirring for 1 h, the suspension was filtered and washed with ultrapure water for three times. Then the resultant powder was redispersed into 20 mL of H_2O through ultra-sonication, and 3.43 mL of freshly prepared $NaBH_4$ aqueous solution (1.0 mg mL^{-1}) was added under stirring for 2 h. The as-synthesized Pd@Cu-TCPP(Fe) was collected through centrifugation and washed with ultrapure water for three times. Finally, the purified Pd@Cu-TCPP(Fe) was dried in a vacuum oven at 60 °C for 12 h, and the yield was about 64.5%.

Exploration of peroxidase–mimic activity of Pd@Cu-TCPP(Fe)

To investigate the peroxidase-like activity of Pd@Cu-TCPP(Fe), the catalytic oxidation was evaluated by using TMB as a chromogenic substrate in the presence of H_2O_2, and UV-vis spectra was used to detect the absorbance at 652 nm. Typically, 40 μL of TMB (5.0 mg mL^{-1}) and 40 μL of H_2O_2 (5.0 mM) were added in 870 μL of sodium acetate buffer (0.2 M, pH 4.0) in the presence of Pd@Cu-TCPP(Fe) (50 μL, 1.0 mg mL^{-1}). The pH-dependent catalytic activity was measured in different reaction buffers (pH 2.4, 3.2, 4.0, 4.5, 5.2, 6.0, 7.0) at 55 °C, while temperature-dependent activity was measured in sodium acetate buffer (0.2 M, pH 4.0) at different temperatures (20, 25, 30, 37, 45, 55, 60, 70 °C). The time-dependent activity was assayed by conducting reaction for 2–10 min, respectively.

Steady-state kinetic analysis of Pd@Cu-TCPP(Fe) was conducted with TMB as chromogenic substrate by using 50 μL of Pd@Cu-TCPP(Fe) (1.0 mg mL^{-1}) dispersion in 870 μL of sodium acetate buffer (0.2 M, pH 4.0) with the same concentration of H_2O_2 (5.0 mM, 40 μL) but different concentrations of TMB (0.5, 0.7, 1.0, 2.0, 3.0, 4.0, 5.0 mg mL^{-1}, 40 μL). Similarly, the kinetic analysis of H_2O_2 as the substrate was performed by using 50 μL of Pd@Cu-TCPP(Fe) (1.0 mg mL^{-1}) dispersion in 870 μL of sodium acetate buffer (0.2 M, pH 4.0) with the same concentration of TMB (5.0 mg mL^{-1}, 40 μL) but different concentrations of H_2O_2 (0.5, 0.6, 0.8, 1.0, 2.0, 3.0, 4.0, 5.0 mM, 40 μL). The initial rates (v_0) of TMB oxidation were determined based on the concentration of oxidized TMB (ox-TMB). The concentration of ox-TMB was calculated by Beer–Lambert law ($A = C_{\text{ox-TMB}} \times \varepsilon_{\text{ox-TMB}} \times b$), in which $\varepsilon_{\text{ox-TMB}}$ was the molar absorption coefficient of ox-TMB (39 000/(mol cm L^{-1}) at 652 nm) and b was the optical length of 1 cm. The Michaelis–Menten equation as followings was employed to explain the catalytic behavior of Pd@Cu-TCPP(Fe), where the Michaelis constant (K_m) and maximum velocity (V_{max}) were extrapolated by plotting the initial rate against the concentration of TMB or H_2O_2.

$$\frac{1}{v_0} = \left(\frac{K_m}{V\max}\right)\frac{1}{[S]} + \frac{1}{V\max}$$

where v_0 is the initial rate of TMB oxidation and $[S]$ is the concentration of substrate. K_m value represents the binding strength between enzyme and substrate, which indicates enzymatic affinity. V_{max} value implies the maximal enzymatic reaction rate.

Colorimetric detection of glucose

In order to validate the applicability of Pd@Cu-TCPP(Fe) catalyst in biological analysis, glucose sensing was carried out through detecting H_2O_2 generated by its corresponding oxidase as follows: firstly, 20 μL of glucose solution with different concentrations (0.2, 0.4, 0.6, 0.8, 1.0, 2.0, 4.0, 6.0, 8.0 mM) was added into 100 μL of sodium acetate buffer (0.2 M, pH 5.2), and after that 20 μL of GOx (1.0 mg mL^{-1}) was added into the above solution. After incubation at 37 °C for 30 min, 770 μL of sodium acetate buffer (0.2 M, pH 4.0), 40 μL of TMB (5.0 mg mL^{-1}) and 50 μL of Pd@Cu-TCPP(Fe) catalyst (1.0 mg mL^{-1}) were subsequently added. After reaction at 55 °C for 5 min, the absorbance of final mixture was measured at room temperature. To investigate the selectivity, lactose, sucrose, maltose, Lys, Trp and HVA with the same concentration of 5.0 mM were all chosen as interferences and the experiment procedure was performed as the same as that of glucose. The reproducibility of this method was assayed by detecting a glucose standard solution (2.0 mM) for six times. In order to evaluate the accuracy of this method, the recovery experiment was performed by spiking glucose standard solutions with different concentrations (0.5 mM, 2.0 mM, 4.0 mM) to the cerebrospinal fluid (CSF). For the glucose detection in human CSF, 100 μL of $ZnSO_4 \cdot 7H_2O$ (0.08 M) was mixed with 100 μL of CSF samples, and then vortexed for 3 min. The mixture was centrifuged at 14 000 rpm for 10 min. The supernatant was collected and used for glucose detection as the aforementioned procedure. This work was approved by the ethics committee of Tongji Hospital, Tongji Medical College, Huazhong University of Science and Technology.

Results and discussion

Characterization of Pd@Cu-TCPP(Fe)

In present work, the synthetic procedure of Pd@Cu-TCPP(Fe) hybrid nanosheets was demonstrated in Scheme 1. The selected 2D MOF, Cu-TCPP(Fe), was constructed by using heme-like TCPP(Fe) as the ligand, Cu clusters as metal nods and PVP as the surfactant. During the preparation of Cu-TCPP(Fe), PVP could attach on the surface of MOF after nucleation, leading to the anisotropic growth of MOF and final formation of ultrathin 2D Cu-TCPP(Fe) nanosheets.[38] Then, PdNPs were decorated on Cu-TCPP(Fe) nanosheets by a simple reduction method under room temperature. The morphology characteristics of as-prepared Pd@Cu-TCPP(Fe) were observed by TEM. The low contrast in TEM images (Fig. 1a) revealed ultrathin features of 2D nanosheets as reported, indicating successful synthesis of Cu-TCPP(Fe) nanosheets.[39] The black dots were PdNPs, and the dispersion of PdNPs was uniform with no signs of aggregation (Fig. 1a).[40] In addition, the average size of PdNPs was about 2.5 nm (Fig. 1b). All these demonstrated the successful *in situ* growth of PdNPs on the surface of Cu-TCPP(Fe) nanosheets, and the smaller size might be helpful for improved activity. The element mappings (Fig. 1c) showed the presence of six elements, including C, N, O, Cu, Fe and Pd. It was also clearly seen that PdNPs were uniformly dispersed, which further supported the TEM results.

The PXRD diffraction patterns was performed to identify the crystalline nature of 2D Cu-TCPP(Fe) and Pd@ Cu-TCPP(Fe) nanosheets (Fig. 1d). The characteristic diffraction peaks at the (110), (002), and (004) planes were well matched with the literature.[15,41] In addition, similar PXRD patterns of Cu-TCPP(Fe) and Pd@ Cu-TCPP(Fe) further indicated that the loading of Pd nanoparticles did not disturb the crystal structure of 2D Cu-TCPP(Fe) nanosheets. The monolayer character of 2D Cu-TCPP(Fe) was visualized by AFM imaging, and the thickness was about 1.7 nm (Fig. 1e) which was similar with that reported in the literature.[41]

FTIR spectrum was used to characterize the product in each reaction step. As shown in Fig. 2a, the absorption at 1620 and

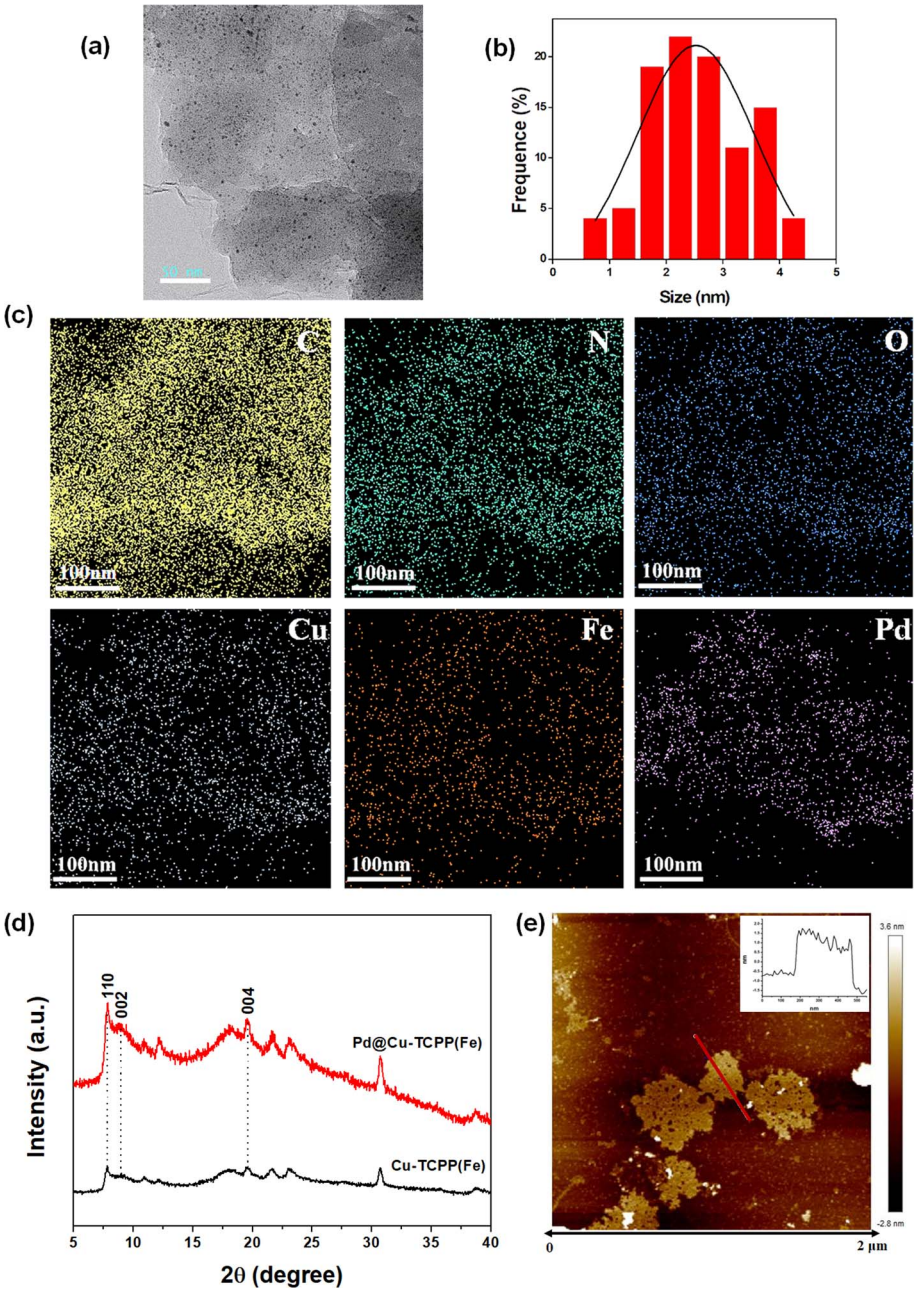

Fig. 1 (a) TEM image of Pd@Cu-TCPP(Fe); (b) particle size distribution of Pd nanoparticles in Pd@Cu-TCPP(Fe); (c) EDS mapping of Pd@Cu-TCPP(Fe); (d) PXRD patterns of 2D Cu-TCPP(Fe) (black) and Pd@Cu-TCPP(Fe) (red); (e) AFM image of 2D Cu-TCPP(Fe) nanosheets.

1400 cm^{-1} indicated the coordination between the carboxyl group in TCPP and Cu atom.[37] The peak at about 1000 cm^{-1} related to Fe–N stretching vibration showed no obvious difference between Cu-TCPP(Fe) nanosheets and Pd@Cu-TCPP(Fe), suggesting that iron-porphyrin structure was intact after the formation of Pd@Cu-TCPP(Fe) hybrids.[39] The peak appearing at the region of 575 cm^{-1} may be due to the Pd–O vibrations, and supported the coordination of oxygen to metal atom,[42] indicating successful decoration of PdNPs on the surface of Cu-TCPP(Fe) nanosheets.

To further examine the chemical structure of Pd@Cu-TCPP(Fe) hybrid nanosheets, XPS spectrum was recorded. The XPS survey spectrum confirmed the existence of C 1s, N 1s, O 1s, Cu 2p, Fe 2p and Pd 3d, respectively (Fig. 2b), which was in line with TEM element mapping. High-resolution Pd 3d XPS region was split into double peaks due to the spin–orbit coupling effect, which corresponded to Pd $3d_{5/2}$ and Pd $3d_{3/2}$ (Fig. 2c). The Pd $3d_{5/2}$ peak at 336.2 eV and the Pd $3d_{3/2}$ peak at 341.3 eV were assigned to Pd (0), while the other double peaks at 338.1 eV and 343.1 eV were related to Pd^{n+}.[43] The Pd^{n+} may be attributed to partial ionization of Pd surface, resulting in the formation of Pd–O bond.[44] The double peak in Pd@Cu-TCPP(Fe) were slightly higher than normal value of Pd $3d_{5/2}$ and Pd $3d_{3/2}$. The shift indicated changed chemical environment of Pd, which might be

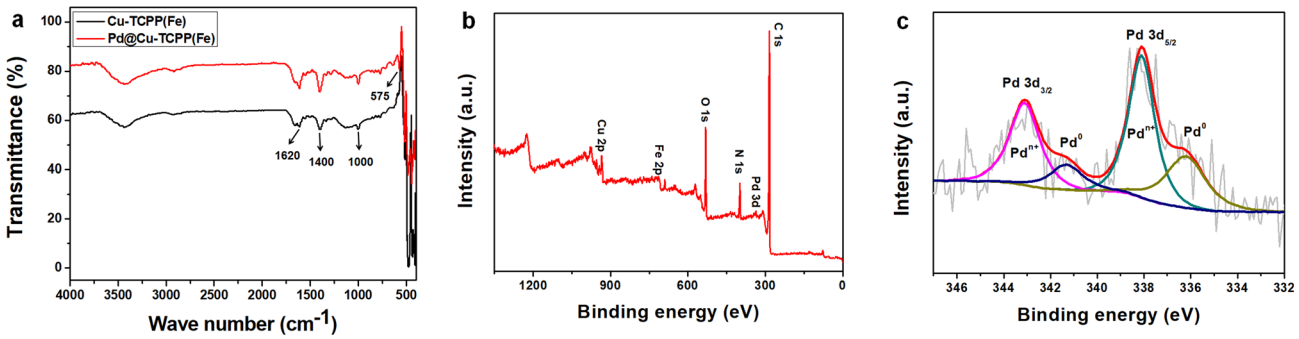

Fig. 2 (a) FTIR spectrum of Cu-TCPP(Fe) and Pd@Cu-TCPP(Fe); X-ray photoelectron of (b) survey spectrum, (c) Pd 3d spectrum of Pd@Cu-TCPP(Fe).

attributed to the fact that Pd could coordinate with other atoms and lost electrons, decreasing the electron density. These changes suggested that Pd@Cu-TCPP(Fe) hybrid nanosheets were not only a mixture of two unrelated compounds but rather were interconnected structure formed by strong metal support interactions or chemical bonds. These physicochemical interactions were beneficial for stability and performance of the hybrids.

Exploration of peroxidase–mimic activity of Pd@Cu-TCPP(Fe)

The peroxidase–mimic activity of Pd@Cu-TCPP(Fe) was explored through the oxidation of TMB into a chromogenic product (ox-TMB) in the presence of H_2O_2. After decorated with PdNPs, a strong UV-vis absorbance at 652 nm was observed in the final reacted mixture, indicating enhanced catalytic property of Pd@Cu-TCPP(Fe) towards TMB oxidation in the presence of H_2O_2 (Fig. 3a). This might be resulted from the synergistic effect between PdNPs and Cu-TCPP(Fe) nanosheets. It has been reported that Cu-TCPP(Fe) nanosheets possess abundant electron transfer channels, larger surface area and more accessible active sites for substrate molecules with a smaller diffusion barrier, resulting in nice catalytic activity as biomimetic enzymes.[15,16] In addition, PdNPs have been reported to exhibit high peroxidase-like catalytic activity due to unique electron configuration and high specific surface area.[33,45] Thus, there

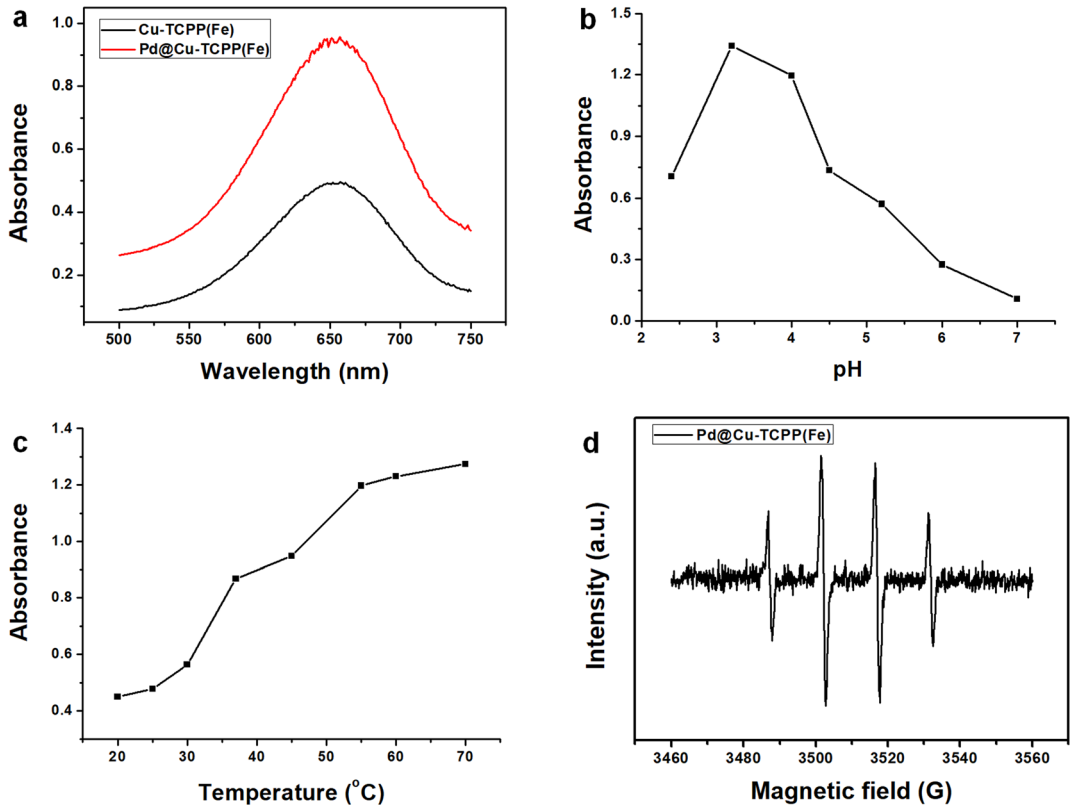

Fig. 3 Exploring of enzymatic activity of Pd@Cu-TCPP(Fe) influenced by (a) PdNPs, (b) pH, (c) temperature; (d) EPR spectrum of Pd@Cu-TCPP(Fe).

might be two possible mechanisms of synergistic effect for improved catalytic activity. On one hand, 2D Cu-TCPP(Fe) nanosheets were favorable for providing electron transfer channels and dispersed adsorption of PdNPs. On the other hand, PdNPs possessed unique electron property favorable for stimulating electron transfer on the surface of 2D MOF nanosheets.

Next, the influence of pH value and reaction temperature on the peroxidase–mimic activity of nanozymes was investigated. As shown in Fig. 3b, the optimal catalytic activity was achieved at pH 3.2 and only a bit decrease was observed at pH 4.0. Moreover, this nanozyme demonstrated obvious catalytic activity in acidic buffer solution (pH 2.4–6.0), but almost no catalytic activity in neutral solution (pH 7.0). This phenomenon could be explained by the fact that weak acid environment is favorable for the transfer of electrons and could accelerate the catalytic oxidation of TMB.[46] In addition, reaction temperature posed great impact on 2D MOF catalytic activity in Fig. 3c. The catalytic activity demonstrated a sharp increase with the temperature elevated from 20 to 70 °C and nearly reached a platform at 55 °C, indicating great influence of temperature. Furthermore, the impact of incubation time on the colorimetric reaction was studied. An obviously positive relationship between absorbance and incubation time ranged from 2 to 5 min was observed, but only a bit elevation from 5 to 10 min (Fig. S1†). All these indicated that, in comparison with soluble horseradish peroxidase (HPR),[47] this nanozyme is more stable and show great catalytic activity under relatively harsh pH or temperature within a short time. Considering the convenience of constructing cascade reaction with natural enzyme, pH 4.0, 55 °C and incubation for 5 min were adopted in the following experiment for rapid detection.

Table 1 K_m and V_{max} of Pd@Cu-TCPP(Fe), HPR and other nanozymes

	K_m (mM)		V_{max} (10^{-8} M s^{-1})		
Catalyst	TMB	H_2O_2	TMB	H_2O_2	Ref.
Pd@Cu-TCPP(Fe)	11.97	2.33	10.31	12.22	This work
HRP	0.434	3.70	10.0	8.71	49
2D Cu-TCPP(Fe)	1.20	9.88	0.98	18.34	21
2D Ni-MOF nanosheet	0.365	2.49	6.53	130	51
Pd NAFs	0.040	13.768	16.89	29.06	50
PtPd NAs/GNs	0.33	13.67	56.87	11.09	30
Pd/N-S-CS	1.44	42.7	24.1	38.9	33
Pd@ZIF-8	0.13	14.02	30.74	27.70	35
Pd@ Schiff base	8.86	1.17	3.72	3.67	34

To characterize the peroxidase-like activity of Pd@Cu-TCPP(Fe) nanosheets, steady-state kinetic assays were performed using TMB and H_2O_2 as substrates. Typical Michaelis–Menten curves were gotten by plotting the initial rate (v_0) against concentrations of TMB (Fig. S2a†) or H_2O_2 (Fig. S2c†) based on Beer–Lambert law.[48] Then, linear transformation of Michaelis–Menten equation was performed by Lineweaver–Burk's method (Fig. S2b and d†). The Michaelis–Menten constant (K_m) and the maximum initial velocity (V_{max}) were calculated from the slope and intercepts of the corresponding linear curves. The K_m and V_{max} values of Pd@Cu-TCPP(Fe) for H_2O_2 were 2.33 mM and 12.22 × 10^{-8} M s^{-1}. A comparison of K_m and V_{max} values between Pd@Cu-TCPP(Fe) and other enzymes was shown in Table 1. In comparison with HPR, other 2D MOFs and other Pd incorporated nanozymes,[21,30,33–35,49–51] PdNPs decorated 2D MOF presented a relative lower *K*m value toward H_2O_2, indicating its higher affinity for H_2O_2 and nice catalytic activity.

To elucidate the catalytic mechanism of Pd@Cu-TCPP(Fe), EPR spectroscopy was performed to confirm the radical intermediates. As demonstrated in Fig. 3d, intense quadruple peak signals for ˙OH with an intensity of 1 : 2 : 2 : 1 were detected, indicating the decomposition of H_2O_2 to produce ˙OH mediated by Pd@Cu-TCPP(Fe). This phenomenon confirmed its peroxidase mimics activity, which was found to be similar with previously reported porphyrin based 2D MOF.[20,52]

Colorimetric detection of glucose

To verify its feasibility in practical application, Pd@Cu-TCPP(Fe) was further used to couple with GOx for quantitative

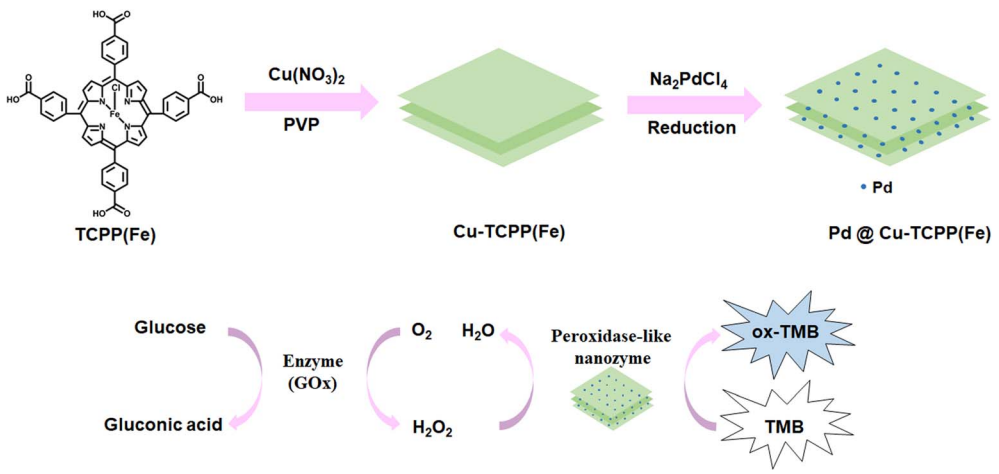

Scheme 1 Schematic illustration of the synthesis of Pd@Cu-TCPP(Fe) and its peroxidase–mimic activity for the detection of glucose.

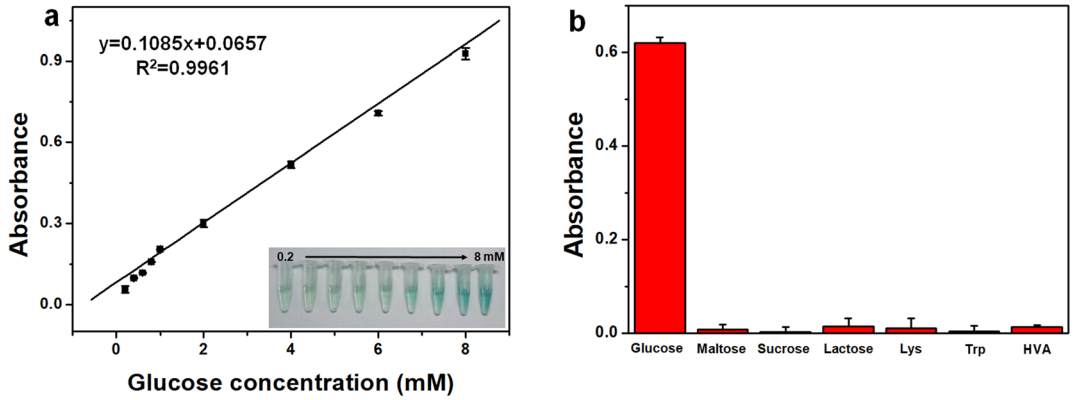

Fig. 4 (a) Linear calibration plot between UV-vis absorbance at 652 nm and glucose concentration in the range of 0.2–8.0 mM, (b) the signal difference between glucose and other interferences (the concentration of each sample was 5.0 mM).

detection of glucose. GOx could convert glucose and oxygen to gluconic acid and H_2O_2, and the reaction between obtained H_2O_2 and TMB could be further catalyzed by Pd@Cu-TCPP(Fe) hybrid nanosheets, forming blue ox-TMB (Scheme 1). As a result, glucose concentration could be measured indirectly by the determination of ox-TMB concentration. As demonstrated in Fig. 4a, the absorbance of ox-TMB at 652 nm (y) has a linear correlation with glucose concentration (x) in the range of 0.2–8.0 mM, which is much appropriate to the reference intervals of glucose in human body.[53] The corresponding linear equation was $y = 0.1085x + 0.0657$ ($R^2 = 0.9961$) and the limit of detection (LOD) was 0.07 mM.

To verify this colorimetric method, the accuracy, reproducibility and selectivity were fully investigated. As shown in Table S1,† three standard samples with different glucose concentration (0.5 mM, 2.0 mM, 4.0 mM) were spiked into the cerebrospinal fluid sample, and the recovery ranged from 89.5%–94.2%, indicating nice accuracy of this method. The sample with glucose concentration of 2.0 mM was tested for six times and the RSD of UV signal was 3.65%, indicating its good reproducibility. Moreover, considering complex components in human matrix, several possible interfering substances, such as maltose, sucrose, lactose, Lys, Trp and HVA, was determined by this colorimetric method based on Pd@Cu-TCPP(Fe) (Fig. 4b). There was no obvious absorbance in the existence of these interfering substances, which would be attributed to the specificity of GOx toward its substrate. Thus, this colorimetric method presented the merits of wide linear range, good accuracy, nice reproducibility and satisfied selectivity.

After valid verification, this colorimetric method based on cascade reaction between GOx and Pd@Cu-TCPP(Fe) was applied to determine glucose in three human cerebrospinal fluid samples. For method comparison, the cerebrospinal fluid samples were also tested on a Cobas 8000 system (Roche, Diagnostics, Germany). The comparable glucose concentrations between these two methods indicated good reliability of this developed colorimetric method (Table 2).

Table 2 The comparison of detection results from this biosensor and the commercial chemical analyzer

No.	This biosensor (mM)	The chemical analyzer (mM)	Accuracy
Sample 1	3.36	3.37	99.7%
Sample 2	4.64	4.34	106.9%
Sample 3	3.06	3.31	92.4%

Conclusions

In conclusion, a novel nanozyme based on Pd@Cu-TCPP(Fe) hybrid nanosheets was proposed. 2D structure of Cu-TCPP(Fe) was verified to be favorable for the formation and immobilization of Pd nanoparticles. The as-synthesized Pd@Cu-TCPP(Fe) hybrid nanosheets exhibited peroxidase-like activity, and the Pd@Cu-TCPP(Fe) mediated reaction was greatly dependent on pH, temperature and reaction time. From the cascade reaction between GOx and Pd@Cu-TCPP(Fe), a quick colorimetric method for determination of glucose in human cerebrospinal fluids was established and verified with satisfying recovery, reproducibility and selectivity. Importantly, the as-prepared Pd@Cu-TCPP(Fe) with peroxidase-like activity exhibits certain merits over natural enzymes, such as easy preparation, low-cost and chemical stability, which paves a new way for finding high-efficient nanozymes based on 2D MOFs. As well, this study offers a newly 2D MOF based colorimetric bioassay for glucose determination, showing its good potential application in clinical diagnosis.

Author contributions

Ying Shen: conceptualization, investigation, data curation, methodology, formal analysis and writing–original draft. Yuanhong Wu: investigation and data curation. Xia Luo: methodology. Haizhi Zhang: conceptualization, resources and supervision. Liming Cheng: project administration and supervision.

Conflicts of interest

The authors declare no competing interests.

Abbreviations

GOx	Glucose oxidase;
Pd	Palladium;
MOFs	Metal–organic frameworks;
TMB	3,3,5′,5′-Tetramethylbenzidine;
2D	Two-dimensional;
TCPP(Fe)	Fe(III) *meso*-tetra (4-carboxyphenyl) porphyrin chloride;
$Cu(NO_3)_2 \cdot 3H_2O$	Copper nitrate trihydrate;
Na_2PdCl_4	Sodium tetrachloropalladate;
PVP	Poly-vinylpyrrolidone;
$NaBH_4$	Sodium borohydride;
H_2O_2	Hydrogen peroxide;
$ZnSO_4 \cdot 7H_2O$	Zinc sulfate heptahydrate;
GO	Glucose;
Lys	Lysine;
Trp	Tryptophan;
HVA	Homovanilic acid;
ox-TMB	Oxidized TMB;
TEM	Transmission electron microscopy;
EDS	Energy dispersive spectroscopy;
XPS	X-Ray photoelectron spectroscopy;
PXRD	Powder X-ray diffraction;
AFM	Atomic force microscopy;
FTIR spectroscopy	Fourier transform infrared spectroscopy;
EPR spectra	Electron paramagnetic resonance spectra;
HRP	Horseradish;
K_m	Michaelis–Menten constant;
V_{max}	Maximum initial velocity

Acknowledgements

The authors greatly appreciate Wuhan Polytechnic University for the support.

References

1 S. Castiglioni, E. Zuccato, E. Crisci, C. Chiabrando, R. Fanelli and R. Bagnati, *Anal. Chem.*, 2006, **78**, 8421–8429.
2 H. H. Noh, S. H. Jo, H. W. Shin, D. J. Kim, Y. J. Ham, J. Y. Kim, D. B. Kim, H. Y. Kwon and K. S. Kyung, *Foods*, 2022, **11**, 416.
3 B. M. Kunz, L. Pförtner, S. Weigel, S. Rohn, A. Lehmacher and R. Maul, *Mycotoxin Res.*, 2022, **38**, 37–50.
4 C. N. Ezekiel, W. A. Abia, D. Braun, B. Šarkanj, K. I. Ayeni, O. A. Oyedele, E. C. Michael-Chikezie, V. C. Ezekiel, B. N. Mark, C. P. Ahuchaogu, R. Krska, M. Sulyok, P. C. Turner and B. Warth, *Environ. Int.*, 2022, **158**, 106996.
5 Y. Shen Y, X. Luo, H. J. Li, Z. J. Chen, Q. Guan and L. M. Cheng, *J. Chromatogr. B: Anal. Technol. Biomed. Life Sci.*, 2020, **1158**, 122395.
6 A. M. Ashrafi, Z. Bytesnikova, J. Barek, L. Richtera and V. Adam, *Biosens. Bioelectron.*, 2021, **192**, 113494.
7 M. M. Liang, K. L. Fan, Y. Pan, H. Jiang, F. Wang, D. L. Yang, D. Lu, J. Feng, J. J. Zhao, L. Yang and X. Y. Yan, *Anal. Chem.*, 2013, **85**, 308–312.
8 X. L. Guo, Y. X. Suo, X. Zhang, Y. S. Cui, S. F. Chen, H. T. Sun, D. W. Gao, Z. W. Liu and L. G. Wang, *Analyst*, 2019, **144**, 5179–5185.
9 S. J. Zhuo, J. Fang, C. Q. Zhu and J. Y. Du, *Anal. Bioanal. Chem.*, 2020, **412**, 963–972.
10 C. Y. Chen, Y. Z. Tan, P. H. Hsieh, C. M. Wang, H. Shibata, K. Maejima, T. Y. Wang, Y. Hiruta, D. Citterio and W. S. Liao, *ACS Sens.*, 2020, **5**, 1314–1324.
11 N. Tao, H. H. Li, L. Deng, S. F. Zhao, J. Ouyang, M. Wen, W. S. Chen, K. Zeng, C. W. Wei and Y. N. Liu, *ACS Nano*, 2022, **16**, 485–501.
12 H. B. Wu, F. Xia, L. X. Zhang, C. Y. Fang, J. Lee, L. J. Gong, J. Q. Gao, D. S. Ling and F. Y. Li, *Adv. Mater.*, 2022, **34**, e2108348.
13 M. Z. Lv, W. Zhou, H. Tavakoli, C. Bautista, J. F. Xia, Z. H. Wang and X. J. Li, *Biosens. Bioelectron.*, 2021, **176**, 112947.
14 L. P. Du, W. Chen, P. Zhu, Y. L. Tian, Y. T. Chen and C. S. Wu, *Biotechnol. J.*, 2021, **16**, e1900424.
15 Y. X. Wang, M. T. Zhao, J. F. Ping, B. Chen, X. H. Cao, Y. Huang, C. L. Tan, Q. L. Ma, S. X. Wu, Y. F. Yu, Q. P. Lu, J. Z. Chen, W. Zhao, Y. B. Ying and H. Zhang, *Adv. Mater.*, 2016, **28**, 4149–4155.
16 Y. Huang, M. T. Zhao, S. K. Han, Z. C. Lai, J. Yang, C. L. Tan, Q. L. Ma, Q. P. Lu, J. Z. Chen, X. Zhang, Z. C. Zhang, B. Li, B. Chen, Y. Zong and H. Zhang, *Adv. Mater.*, 2017, **29**, 1700102.
17 L. Qin, X. Y. Wang, Y. F. Liu and H. Wei, *Anal. Chem.*, 2018, **90**, 9983–9989.
18 H. Y. Chen, Q. M. Qiu, S. Sharif, S. N. Ying, Y. B. Ying and Y. X. Wang, *ACS Appl. Mater. Interfaces*, 2018, **10**, 24108–24115.
19 X. Y. Wang, X. Q. Jiang and H. Wei, *J. Mater. Chem. B*, 2020, **8**, 6905–6911.
20 H. Y. Yang, Z. P. Sun, X. G. Qin, H. Y. Wu, H. Z. Zhang and G. Liu, *Food Chem.*, 2022, **376**, 131906.
21 H. Z. Zhang, H. Y. Yang, P. Liu, X. G. Qin and G. Liu, *Talanta*, 2022, **237**, 122906.
22 L. J. Wang, S. E. Saji, L. J. Wu, Z. X. Wang, Z. J. Chen, Y. P. Du, X. F. Yu, H. T. Zhao and Z. Y. Yin, *Small*, 2022, **18**, e2201642.
23 C. Y. Guo, Y. H. Zhang, L. Zhang, Y. Zhang and J. D. Wang, *CrystEngComm*, 2018, **20**, 5327–5331.
24 J. J. Wu, X. Y. Wang, Q. Wang, Z. P. Lou, S. R. Li, Y. Y. Zhu, L. Qin and H. Wei, *Chem. Soc. Rev.*, 2019, **48**, 1004–1076.
25 M. Azharuddin, G. H. Zhu, D. Das, E. Ozgur, L. Uzun, A. P. F. Turner and H. K. Patra, *Chem. Commun.*, 2019, **55**, 6964–6996.
26 T. T. V. Phan, T. C. Huynh, P. Manivasagan, S. Mondal and J. Oh, *Nanomaterials*, 2020, **10**, 66.
27 Y. Nangia, B. Kumar, J. Kaushal and C. R. Suri, *Anal. Chim. Acta*, 2012, **751**, 140–145.
28 A. Mohamad, M. Rizwan, N. A. Keasberry, A. S. Nguyen, T. D. Lam and M. U. Ahmed, *Biosens. Bioelectron.*, 2020, **155**, 112108.

29 Z. Dehghani, M. Hosseini, J. Mohammadnejad, B. Bakhshi and A. H. Rezayan, *Mikrochim. Acta*, 2018, **185**, 448.
30 X. M. Chen, Z. X. Cai, X. Chen and M. Oyama, *J. Mater. Chem. A*, 2014, **2**, 315–320.
31 W. Li, X. Zhi, J. J. Yang, J. L. Zhang and Y. Fu, *Anal. Methods*, 2016, **8**, 5111–5116.
32 Y. Fu, H. X. Zhang, S. D. Dai, X. Zhi, J. L. Zhang and W. Li, *Analyst*, 2015, **140**, 6676–6683.
33 W. J. Shi, H. Fan, S. Y. Ai and L. S. Zhu, *RSC Adv.*, 2015, **5**, 32183–32190.
34 K. Y. Wang, K. Chen, T. J. Prior, X. Feng and C. Redshaw, *ACS Appl. Mater. Interfaces*, 2022, **14**, 1423–1433.
35 Y. Li, S. J. Li, M. Bao, L. Q. Zhang, C. Carraro, R. Maboudian, A. R. Liu, W. Wei, Y. J. Zhang and S. Q. Liu, *ACS Appl. Nano Mater.*, 2021, **4**, 9132–9142.
36 Z. G. Gao, L. Hou, M. D. Xu and D. P. Tang, *Sci. Rep.*, 2014, **4**, 3966.
37 R. Rahimi, S. Shariatinia, S. Zargari, M. Y. Berijani, A. Ghaffarinejad and Z. S. Shojaie, *RSC Adv.*, 2015, **5**, 46624.
38 M. T. Zhao, Y. X. Wang, Q. L. Ma, Y. Huang, X. Zhang, J. F. Ping, Z. C. Zhang, Q. P. Lu, Y. F. Yu, Y. L. Zhao and H. Zhang, *Adv. Mater.*, 2015, **27**, 7372–7378.
39 P. Wu, X. S. Ye, D. Q. Wang, F. J. Gong, X. Q. Wei, S. Xiang, J. W. Zhang, T. H. Kai and P. Ding, *J. Hazard. Mater.*, 2022, **424**, 127690.
40 Y. Zhang, R. Guo, D. N. Wang, X. T. Sun and Z. R. Xu, *Colloids Surf., B*, 2019, **176**, 300–308.
41 H. J. Cheng, Y. F. Liu, Y. H. Hu, Y. B. Ding, S. C. Lin, W. Cao, Q. Wang, J. J. X. Wu, F. Muhammad, X. Z. Zhao, D. Zhao, Z. Li, H. Xing and H. Wei, *Anal. Chem.*, 2017, **89**, 11552–11559.
42 T. Kumari, R. Gopal, A. Goyal and J. Joshi, *J. Inorg. Organomet. Polym. Mater.*, 2019, **29**, 316–325.
43 J. Z. Li and X. F. Bai, *J. Mater. Sci.*, 2016, **5**, 9108–9122.
44 P. Chandran, A. Ghosh and S. Ramaprabhu, *Sci. Rep.*, 2018, **8**, 3591.
45 C. Egan-Morriss, R. L. Kimber, N. A. Powell and J. R. Lloyd, *Nanoscale Adv.*, 2022, **4**, 654.
46 M. M. Chen, B. C. Yang, J. L. Zhu, H. Liu, X. Zhang, X. W. Zheng and Q. Y. Liu, *Mater. Sci. Eng., C*, 2018, **90**, 610–620.
47 S. A. Mohamed, M. H. Al-Harbi, Y. Q. Almulaiky, I. H. Ibrahim and R. M. EI-Shishtawy, *Electron. J. Biotechnol.*, 2017, **27**, 84–90.
48 F. Wei, X. Y. Cui, Z. Wang, C. C. Dong, J. D. Li and X. J. Han, *Chem. Eng. J.*, 2021, **408**, 127240.
49 L. Z. Gao, J. Zhuang, L. Nie, J. B. Zhang, Y. Zhang, N. Gu, T. H. Wang, J. Feng, D. L. Yang, S. Perrett and X. Y. Yan, *Nat. Nanotechnol.*, 2007, **2**, 577–583.
50 W. D. Liu, J. N. Guo, C. X. Chen, P. J. Ni, Y. Y. Jiang, C. H. Zhang, B. Wang and Y. Z. Lu, *Mikrochim. Acta*, 2021, **188**, 114.
51 J. Y. Chen, Y. Shu, H. L. Li, Q. Xu and X. Y. Hu, *Talanta*, 2018, **189**, 254–261.
52 Y. Wang, Y. Xue, Q. L. Zhao, S. Wang, J. Sun and X. R. Yang, *Anal. Chem.*, 2022, **94**, 16345–16352.
53 W. G. Leen, M. A. Willemsen, R. A. Wevers and M. M. Verbeek, *PLoS One*, 2012, **7**, e42745.